Active multistage coarsening of actin networks driven by myosin motors

Marina Soares e Silva[a], Martin Depken[b], Björn Stuhrmann[a], Marijn Korsten[a], Fred C. MacKintosh[b], and Gijsje H. Koenderink[a,1]

[a]Foundation for Fundamental Research on Matter Institute for Atomic and Molecular Physics (FOM Institute AMOLF), 1009 DB, Amsterdam, The Netherlands; and [b]Vrije Universiteit Amsterdam, 1081 HV, Amsterdam, The Netherlands

Edited by Paul A. Janmey, University of Pennsylvania, Philadelphia, PA, and accepted by the Editorial Board April 21, 2011 (received for review November 6, 2010)

In cells, many vital processes involve myosin-driven motility that actively remodels the actin cytoskeleton and changes cell shape. Here we study how the collective action of myosin motors organizes actin filaments into contractile structures in a simplified model system devoid of biochemical regulation. We show that this self-organization occurs through an active multistage coarsening process. First, motors form dense foci by moving along the actin network structure followed by coalescence. Then the foci accumulate actin filaments in a shell around them. These actomyosin condensates eventually cluster due to motor-driven coalescence. We propose that the physical origin of this multistage aggregation is the highly asymmetric load response of actin filaments: they can support large tensions but buckle easily under piconewton compressive loads. Because the motor-generated forces well exceed this threshold, buckling is induced on the connected actin network that resists motor-driven filament sliding. We show how this buckling can give rise to the accumulation of actin shells around myosin foci and subsequent coalescence of foci into superaggregates. This new physical mechanism provides an explanation for the formation and contractile dynamics of disordered condensed actomyosin states observed in vivo.

active gels | molecular motors | nonequilibrium | soft condensed matter

Cells undergo dramatic changes in shape and internal organization during vital processes such as migration and division. These changes involve remodeling of the cytoskeleton partly driven by collective physical interactions between molecular motors and cytoskeletal filaments. The motors use adenosine triphosphate (ATP) as fuel and hydrolyze it to actively generate forces and move along filaments (1). Multiheaded motors or complexes of motors may cross-link neighboring filaments and generate relative motion between them. Kinesin and dynein motors interact with microtubules to form the mitotic spindle, which is responsible for chromosome segregation (2). Myosin motors interact with filamentous actin (F-actin) to form complex arrays such as the contractile ring driving cell division (3, 4) and contractile networks that drive cell migration (4) and polarizing cortical flows (5, 6).

To identify the biophysical processes underlying cytoskeletal organization, many in vitro model systems of purified motors and filaments that lack biochemical regulation have been recently developed. It is known that kinesins can organize microtubules into polarity sorted asters, as well as vortex or bundle states (7–10). These structures resemble physiological arrays such as the mitotic spindle (11). In contrast to microtubules, purified F-actin does not form well-defined structures when motors are added. Actin-myosin II solutions remain disordered at high levels of ATP (12–14) and generate dense condensates that appear internally unstructured if the ATP level is lowered or when the actin filaments are cross-linked (15–18). Interestingly, similar dense condensates appear in cells during myosin-driven shape changes of the actin cytoskeleton. Formation of the contractile ring in dividing fibroblasts (19) and *Caenorhabditis elegans* embryos (20) both involve large-scale flows and coalescence of dense actomyosin condensates. Similarly, the lamellipodium of migrating cells displays dense myosin aggregates (21, 22). Wounded cells display similar phenomena, with accumulation of myosin foci at the wound border and fusion of these foci into a tight ring capable of constriction (23). Collective shape changes in epithelial cell layers also seem to be driven by the transient formation of myosin spots that subsequently fuse (24–27).

The physical mechanism of self-organization in the actin-myosin cytoskeleton remains unknown. There are several theoretical models describing pattern formation in motor-filament systems (7, 28). These models predict the emergence of ordered aster, vortex, and bundle architectures due to polarity sorting that relies on unidirectional motion of motors along the filaments they connect. Such patterns are also predicted from symmetry considerations, resulting in general hydrodynamic theories of active polar gels (29–31). These patterns are consistent with experimental observations in microtubule-kinesin mixtures (7, 8), but are different from the disordered condensed states seen in actin-myosin mixtures. Microscopic theories model the filaments as rigid and the motors as small, highly processive clusters. Microtubules are indeed rigid and nearly rodlike (32), and their associated motors tend to be highly processive (1), explaining the success of the proposed models in elucidating experimental observations. Unlike kinesins, most myosins are not processive and must act together in large macromolecular assemblies of several tens to hundreds of molecules (33). In addition to the difference in motor processivity, F-actin is 1,000-fold less rigid than microtubules and is known to buckle under compressive loads of fractions of a piconewton (32, 34). In densely cross-linked networks, these microscopic features suggest that the collective organization of myosin and actin into force-generating cellular machines is not driven by polarity sorting but by a different organizing mechanism.

Here we use a model system of purified actin and myosin to uncover the physical mechanism by which myosin motors organize F-actin into contractile structures. We demonstrate that myosin actively drives a multistage coarsening process that brings actin filaments into disorganized condensates that resemble structures seen in vivo. We suggest a microscopic mechanism that can explain this multistage process in terms of buckling of the actin network under the random internal forces generated by motors in such an isotropic structure. This mechanism is fundamentally different from polarity sorting mechanisms operating in microtubule/kinesin systems (7, 8). Furthermore, this mechanism

Author contributions: M.S.e.S., F.C.M., and G.H.K. designed research; M.S.e.S., M.D., B.S., and M.K. performed research; M.S.e.S., M.D., and B.S. analyzed data; and M.S.e.S., M.D., F.C.M., and G.H.K. wrote the paper.

The authors declare no conflict of interest.

This article is a PNAS Direct Submission. P.A.J. is a guest editor invited by the Editorial Board.

[1]To whom correspondence should be addressed. E-mail: g.koenderink@amolf.nl.

This article contains supporting information online at www.pnas.org/lookup/suppl/doi:10.1073/pnas.1016616108/-/DCSupplemental.

depends crucially on the open meshwork structure of actin networks, which is not well captured by continuum mechanical modeling that is frequently applied in active gel theories at larger scales (35–37).

Results

To examine how actin filament reorganization emerges from the collective activity of molecular motors, we reconstituted a minimal model system from purified proteins. F-actin was polymerized from monomers at a 1 mg/mL concentration to form homogeneous networks with no preferred filament orientation or polarity. To generate active internal stresses, we added skeletal muscle myosin II. Myosin II has two identical head domains with binding sites for actin filaments and ATP, and a coiled-coil tail domain (1). Individual myosin motors are nonprocessive: they release immediately after taking one step toward the plus end of an actin filament. However, multiple myosins can assemble tail-to-tail into bipolar filaments with motor heads at each end (in green, Fig. 1*D*) (38). Such assemblies have an increased collective duty cycle, allowing them to transiently cross-link actin filaments (in red, Fig. 1*D*). Moreover, their bipolar geometry enables myosin heads to pull actin filaments of opposite orientations toward each other, as shown by the arrows. We used myosin filaments with an average length of 0.69 μm (Fig. 1*E*) or approximately 100 myosin motors (39). This size is larger than the size of myosin minifilaments in nonmuscle cells, which have 10–30 motors (21, 22). A test with minifilaments of approximately 16 skeletal muscle myosins showed little effect on actin filament reorganization (Fig. S1 *A*–*C*). However, we expect that minifilaments of nonmuscle myosin, in particular myosin IIB, will be more processive because this myosin has a higher duty ratio than its muscle counterpart (Table S1).

Active self-organization was initiated by polymerizing actin in the presence of preformed myosin filaments and 100 μM ATP. Motor activity was kept constant by an enzymatic ATP regeneration system (16). To enable observation of the network structure by microscopy, we fluorescently labeled actin and myosin. Within 2 min after mixing, actin was polymerized into a homogeneous network (red in Fig. 1*A i*). The myosin filaments were initially homogeneously dispersed in the network (green dots indicated by arrow). However, after about 5 min, the myosin was redistributed into bright foci (green in Fig. 1*A ii*). The F-actin network was still homogeneous (Fig. 1*A iii*). After about 30 min, the myosin foci were surrounded by actin rings (red in Fig. 1*B i*). These rings are reminiscent of actin rings observed in the presence of skeletal myosin minifilaments and the actin bundler fascin (40). However, high-resolution images of the rings with only actin fluorescently labeled (to avoid spectral crosstalk with myosin) revealed that they were not composed of a continuous band of actin filaments, but rather of a collection of compact actin aggregates with a size below 1 μm (Fig. 1*B ii*, red arrow). The rings were surrounded by a diffuse halo of actin filaments that radiated outward (Fig. 1*B ii*, white arrow). Three-dimensional image stacks further revealed that, rather than forming flat rings, actin deposited in a shell all around the myosin foci (Movie S1 and Fig. S2*A*). These actin-myosin condensates were initially isolated structures within the actin network, but after 30–45 min we observed larger structures that appeared to be aggregates of actomyosin condensates (Fig. 1*C i*). High-resolution images showed that each aggregate consisted of a few hollow actin rings stuck together (Fig. 1*C ii*). Three-dimensional image stacks showed that these actin rings were again not flat, but that actin formed shells around the myosin foci (Movie S2). Each aggregate contained several myosin foci with actin intercalated between them (Fig. S2*B*), suggesting that they result from coalescence of multiple actomyosin condensates.

These observations suggest that myosin motors drive coalescence of actin into disordered aggregates through a multistage process. To elucidate the transition pathway between these stages, we studied the dynamics of the myosin motors and the actin network in each stage by time-lapse imaging.

In the first stage, the myosin filaments were homogeneously distributed in the network. We tracked the filaments over time and found that they were strikingly mobile (Fig. 2*A* and Movie S3). Many filaments moved by a sequence of straight runs, punctuated by abrupt changes in direction. The long run lengths indicate the motors were not simply diffusing in solution, but moved on the F-actin network. Occasionally, two neighboring myosin filaments came together and fused into a small myosin focus (Fig. 2*B* and Movie S4). Upon meeting, small foci sometimes coalesced further into larger myosin foci (Fig. 2*C* and Movie S5). Once the myosin foci reached a size similar to the average pore size (300 nm), they no longer moved because their motion was presumably hindered by the actin mesh. Nonetheless, they could still grow by coalescence with smaller mobile aggregates.

Initially, myosin foci formation did not drastically reshape the actin network (sketched in Fig. 1*A iv*). However, once myosin foci

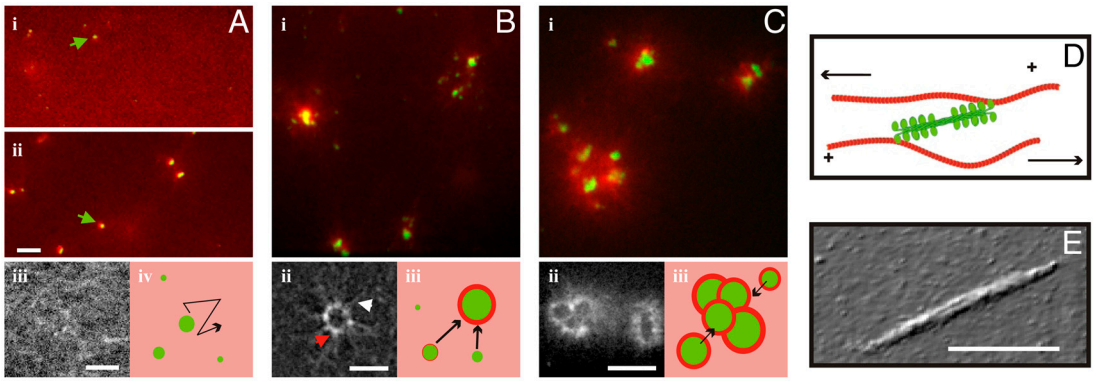

Fig. 1. Actin-myosin networks self-organize through a three-stage coalescence process. (*A*) (*i*) Fluorescence micrograph of an active network, taken 2 min after initiating actin polymerization in the presence of myosin bipolar filaments (1 : 200 myosin : actin). The actin network is homogenous and isotropic (red) and randomly cross-linked by active motors (green). (*ii*) After 6 min, the motors accumulate in larger structures (scale bar 10 μm). (*iii*) The actin network is still homogeneous in this stage. Scale bar 5 μm. (*iv*) In Stage 1 the actin network is homogeneous (pink) and contains small myosin foci (green) that move along the actin network (black arrow). (*B*) (*i*) After 30 min, the actin network is organized in thin shells (red) around myosin foci (green). (*ii*) High-resolution image of an actomyosin condensate shows that actin filaments form a ring-like set of patches (red arrow) with actin filaments radiating out (white arrow). Scale bar 5 μm. (*iii*) In Stage 2, myosin foci are surrounded by thin actin shells and small foci move toward larger immobile foci (arrows). (*C*) (*i*) After 45 min, actomyosin condensates are packed in large superstructures. (*ii*) High-resolution image of a superstructure, showing merged actin ring-like structures. Scale bar 10 μm. (*iii*) In Stage 3, superaggregates form by contractile coarsening (black arrows). (*D*) Network activity results from bipolar myosin filaments (green) sliding actin filaments (red) of opposite orientation toward one another (arrows). (*E*) AFM image of a myosin filament. Scale bar 0.5 μm.

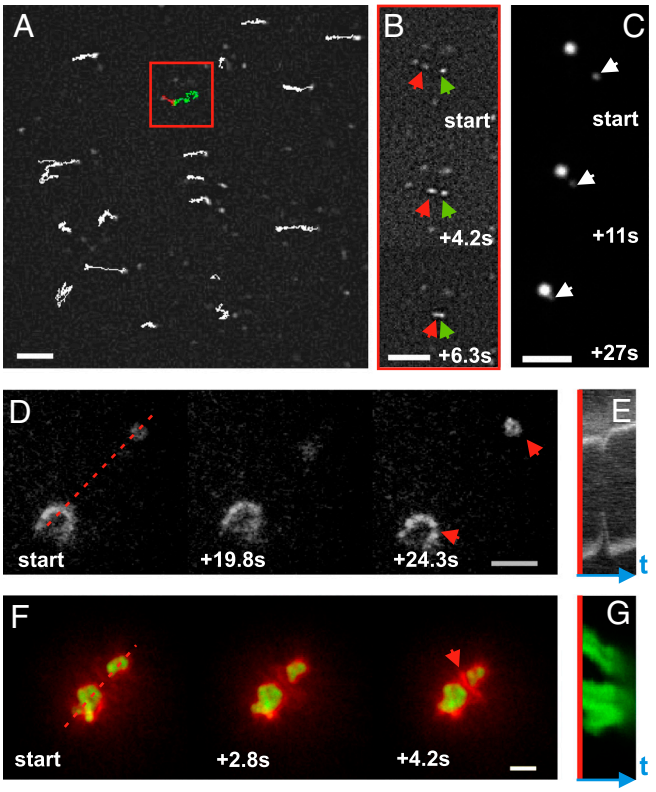

Fig. 2. Dynamics of actin/myosin coalescence. (*A*) Trajectories of myosin filaments moving on an actin network (1:200 myosin:actin; 3 min after sample preparation). Red and green traces represent two filaments that coalesce after an active walk. Scale bar 5 μm. (*B*) Time-lapse image sequence of coalescing myosin filaments corresponding to the green and red traces (see arrows). (*C*) Time-lapse image sequence of two fusing myosin foci. (*D*) Time-lapse image sequence of two actomyosin condensates (red arrows, actin labeled) undergoing a contractile fluctuation (1:200 motors). Scale bar, 10 μm. (*E*) Kymograph constructed along red dashed line in (*D*). (*F*) Time-lapse image sequence of two actomyosin aggregates that coalesce and accumulate actin between them (red arrow, 1:50 myosin:actin). Scale bar, 10 μm. (*G*) Kymograph constructed along red dashed line in (*F*).

became immobile, they were able to capture actin from the surrounding network (Movies S6 and S7). Such events account for the deposition of dense actin patches on the surface of the myosin foci (Fig. 1*B iii*).

The condensation of actin into shells around myosin foci was typically complete within 30 min. Yet, the networks continued to display striking manifestations of contractile activity. Often, two neighboring actomyosin condensates were suddenly pulled toward one another and then recoiled. An example of such a contractile fluctuation event is displayed in Fig. 2*D* (see Movie S8 and Fig. S3*A*, *Upper*). Usually we observed only one recoil, but sometimes recoils occurred twice (Movie S9 and Fig. S3*A*, *Lower*) or even three times (Movie S10 and Fig. S3*B*). Kymographs show that the actin condensates approach and recoil at velocities of approximately 0.3 μm/s (Fig. 2*E*). The myosin foci apparently build up tension over a processivity time window of several tens of seconds, until they unbind from the F-actin leading to an abrupt release of the built-up elastic stress. These observations are consistent with prior indirect observations of contractile network fluctuations based on motions of embedded probe particles (16, 41). Especially at larger motor densities, contraction often resulted in permanent coalescence, likely reflecting the dissipation of elastic stresses before the motors disengage. An example of such a coalescence event is displayed in Fig. 2*F*, where two myosin foci (green) approach each other (Fig. 2*G*) and compact the actin (red) between them (Movie S11). Surprisingly, myosin foci were able to attract each other over distances of up to 25 μm, about five times the average length of the actin filaments. This observation suggests that the actin network between myosin foci is sufficiently connected by myosin cross-links to mediate long-range force transmission. Because the network is disordered on this scale (tens to hundreds of mesh sizes), it is unlikely that filament polarity is the main origin of the directed motion. In a few cases, we observed cable-like actin structures between actomyosin foci that shortened over time (see Movie S12). Contractile coalescence continued until the resulting clusters were too far apart to interact (Fig. 1*C iii*). This final state was typically reached within 100 min.

The extent of aggregation strongly depended on motor density. Higher motor densities increased the probability of irreversible coalescence. At a myosin:actin ratio of 1:200, only half of the contractile events ($N = 55$) resulted in permanent coalescence, whereas at a myosin:actin ratio of 1:50 most events ($N = 29$) resulted in permanent coalescence (Fig. S3*C*). Accordingly, the final steady state at low motor density showed small isolated foci (1:300 and 1:200 in Fig. 3*A*), whereas high motor densities resulted in large superaggregates (1:50 in Fig. 3*A*). To quantify this enhanced tendency for coalescence at high motor densities, we measured the overall size of actin aggregates in steady state. The average size increased from 1.8 μm at low (1:300) myosin:actin ratio to 5.3 μm at high (1:50) myosin:actin ratio (Fig. 3*B* and Table S2). As shown in the insets, this larger size was caused by an increased number of myosin foci at the aggregate core, whereas the thickness of the actin shell remained constant.

The increasing tendency for coarsening with rising motor density is probably the combined outcome of a larger contractile driving force and larger connectivity due to motor cross-linking.

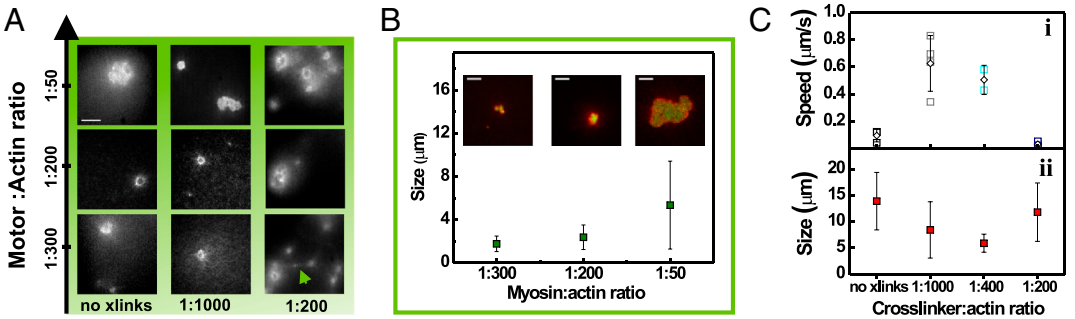

Fig. 3. Active coarsening is promoted by increased motor and cross-link density. (*A*) Steady-state actin patterns observed in active networks containing varying concentrations of myosin motors and biotin-streptavidin cross-links. Scale bar, 10 μm. (*B*) The average size of actomyosin condensates increases with increasing motor density (1:400 biotin:actin). (*Inset*) Confocal images show that this size increase results from an increased degree of coalescence. Scale bars 5 μm. (*C*) (*i*) The average speed of foci movement depends nonmonotonically on cross-link density (actin:myosin ratio 1:50). Open squares represent individual data points; open diamonds represent the average speed for each cross-linker density. (*ii*) The cross-linker density-dependence of the size of actomyosin condensates mirrors that of the contraction speed. All error bars represent SD.

We assessed the effect of network connectivity on contractility by adding passive cross-linkers. F-actin was doped with varying amounts of biotin-actin and cross-linked with streptavidin at a fixed streptavidin:actin ratio (1:25). Biotin-streptavidin cross-links are near-permanent, generating elastic behavior on time scales that are long compared to the lifetime of myosin-actin attachments. We used low cross-link densities to ensure a homogeneous actin network structure (Fig. S4*A*) and prevent macroscopic contraction (15, 17). In the presence of cross-linkers, actin again formed patches around myosin foci, and the resulting actomyosin condensates coalesced. However, coalescence occurred at much lower motor density (myosin:actin ratio 1:200) than in the absence of cross-linkers (1:50) (Fig. 3*A*). This confirms our hypothesis that increased network connectivity promotes contractile coarsening. Interestingly, adding cross-links also influenced the coalescence dynamics. In the absence of cross-links, merging foci had velocities of approximately 0.10 μm/s (Fig. 3*C i* and Table S2). Cross-linking substantially increased the velocity, to a maximum of approximately 0.6 μm/s at a biotin:actin ratio of 1:1000. However, at high cross-linker densities (1:200) the velocity fell back to 0.03 μm/s. The size of the actomyosin condensates showed a reverse dependence on cross-linking, with smallest sizes where the coalescence speed was highest (Fig. 3*C ii* and Table S2). We expect that increasing network connectivity leads to a trade-off between a higher velocity as a greater fraction of filaments is connected to others, and a decreased velocity as the passive stress opposing the active contraction increases. In the most cross-linked networks, the foci were connected by bundle-like actin structures (green arrow in last panel of Fig. 3*A*). Whereas these structures probably facilitate contraction, they are likely connected to the background actin network, thus impeding coalescence.

Discussion

Based upon fluorescence microscopy of active actin/myosin networks, we conclude that myosin drives the formation of disordered actomyosin condensates through a multistage coarsening process. Actin filaments are compacted into dense clouds around large myosin foci and these actomyosin condensates then contract into larger superaggregates. The resulting structures are intrinsically three-dimensional (3D), in strong contrast to the more two-dimensional (2D) aggregates reported previously, such as rings formed in fascin-bundled actomyosin systems (40) and vortices formed in actomyosin networks on surfaces (42). Although planar ring structures might relate to the vortex-like states predicted by active gel theories (29, 31, 43), such features are intrinsically 2D patterns and are topologically not possible in 3D (44). Thus, the nonplanar, shell-like structures we observe must form by another mechanism.

In most active gel theories, the driving force for self-organization comes from small, processive motors or motor clusters. By contrast, we find that large motor assemblies drive the active remodeling in this actin/myosin system. Myosin motor filaments spontaneously form foci, beginning from a uniform distribution in an isotropic actin network. Motors and small motor foci perform random walks on the network: they bind to actin filaments, move along and switch between them, coalescing as they meet (Stage 1, Fig. 4*A*). The apparent, large-scale diffusion constant of this process should be $D \approx vl \approx 1\ \mu m^2/s$. Here $v \approx 1\ \mu m/s$ is the typical speed of myosin aggregates and $\ell \approx 1\ \mu m$ is the typical run length between direction changes, set to be somewhat larger than the mesh size. Because we expect the internal dynamics of the myosin load cycle to be rate limiting, D should be insensitive to aggregate size. As the foci grow to a size comparable to the mesh size of the network, however, their motion will be impeded by elastic interactions with the network. The accumulation of motor filaments into foci occurs without significant concurrent F-actin transport. This differs from self-organization in mixtures of microtubules and kinesin oligomers, where the motors accumulate into foci as they focus microtubules into radial arrays (8, 9).

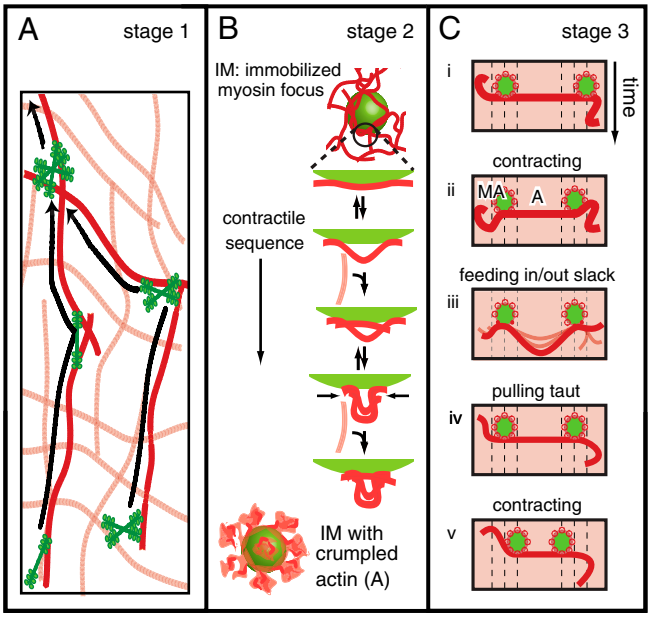

Fig. 4. Proposed multistage mechanism of myosin-driven self-organization of actin networks. (*A*) Stage 1: Myosin filaments or aggregates thereof, move actively on the actin network and coalesce upon meeting. (*B*) Stage 2: An immobilized myosin focus (IM) accumulates a cloud of actin patches in a stochastic sequence of expansive steps (resulting in marginal extension) and contractile steps (resulting in buckling, made permanent by subsequent bridging). The myosin foci have a large interaction surface with the surrounding actin via the protruding myosin heads. Compressive forces exerted by the focus cause the actin to buckle at the surface and form a crumpled actin structure (*A*). (*C*) Stage 3: Two actomyosin aggregates (MA, in green) interact isotropically with the background actin network (shaded red) and will move together by interacting via a connected cluster of actin filaments (represented by a red line). This contraction involves net extension of the connecting actin structure, which brings the foci together, followed by net contraction, which pushes in slack due to buckling. Slack needs to be pulled out before the foci can move closer together.

Once the myosin foci reach a certain size, they initiate Stage 2 of the assembly process by drawing actin in. Due to the random directions of actin filaments in an isotropic network, the net force exerted by a myosin focus [Fig. 4*B*, immobilized myosin focus (IM)] should grow as $N^{1/2}$, where N is the number of actin filaments it interacts with. Eventually, the net force should be sufficient to overcome elastic constraints and perform dissipative work remodelling the local network structure. Collectively, the myosin heads projecting from each focus can exert either an expansive or a compressive force on the surrounding network of actin filaments. We propose that stochastic alternations between expansion and compression will have the net effect of pulling in actin toward a myosin focus (Fig. 4*B*). The physical argument is that actin filaments have a highly asymmetric response to axial loading: They strongly resist stretching but not compression. Under compression, an actin segment of length L readily buckles at a critical force $f_c \sim \pi^2 k_B T \ell_p / L^2$, where the persistence length $\ell_p \sim 17\ \mu m$ (32). For a segment of micrometer length or longer, this force is less than 1 pN (34). The internal forces generated by a single myosin filament already well exceed this buckling threshold (16, 35). Thus, a net expansive force over a patch of actin connected to a myosin focus will be strongly opposed by the high stretch modulus of the actin filaments within the patch. By contrast, a net compressive force will buckle the actin filaments, drawing actin in. This mechanical asymmetry is necessary and sufficient for actin to accumulate, as detailed in *SI Text*, *Contractility from Asymmetric Load Response*. Bridging of buckled structures

by (transient) myosin cross-linking to other actin filaments will further enhance this accumulation [Fig. 4*B*, IM surrounded by crumpled actin (A)].

In the final stage of the coalescence process (Stage 3), actomyosin condensates coalesce into large superaggregates. We propose that if two myosin foci happen to exert forces on the same connected cluster of actin filaments, they will eventually coalesce, again due to the asymmetric load response of actin filaments. If the net forces of the two foci happen to stretch the connecting actin structure, its resistance to extension will force the foci together (Fig. 4*C ii*). If the net forces of the two foci instead happen to compress the connecting actin structure, it will buckle and push in slack between the two foci rather than bearing the load and pushing them apart (Fig. 4*C iii*). Before the random forces can pull the aggregates together again (Fig. 4*C v*), any material buckled during prior compressive loads must be pulled out (Fig. 4*C iv*). Only when the connecting structure is taut can it exert significant forces on the foci. Then the myosin foci will tend to be driven toward each other. Instead of the coherent, unidirectional motion normally associated with motor transport, this model predicts that foci will move in an incoherent, intermittent fashion (*SI Text* and Movie S13). The time-dependent motion of coalescing foci is consistent with this prediction (Fig. S5*E*).

The physical mechanism for actomyosin self-organization outlined above differs substantially from prior models of self-organization in active gels. The nonlinear buckling events that are crucial in our mechanism cannot be captured by linear hydrodynamic theories (29–31, 43) and hitherto have not been part of microscopic theories (36, 45) or simulations (7, 28, 43). Both hydrodynamic and microscopic theories were inspired by experiments in microtubule/kinesin systems (7, 8, 10). These systems differ from actin/myosin systems in at least two aspects. First, microtubules have a persistence length of several millimeters (32) and are therefore not buckled by motor-driven forces. We expect that bundling F-actin should bring the system closer to microtubule systems. Indeed some experimental work points to this: In actomyosin systems bundled by fascin, the final steady states are networks of asters reminiscent of microtubules organized by kinesins (40). In vivo, actin asters with dense clusters of myosin at their center were observed in fibroblasts stimulated to contract with cytochalasin D (46). Such asters had a uniform polarity with actin plus-ends pointing inward, as expected in case of polarity sorting by plus-end directed motors. Second, force centers in active microtubule gels were small, processive motor clusters interacting mostly with microtubule pairs, whereas the force centers in active actin gels are large myosin aggregates interacting with many actin filaments. At a large scale, these force centers can be modeled as force dipoles in a continuum (visco)elastic background. However, on the micrometer scale on which actin reorganizes in our experiments, it is unlikely that continuum elasticity represents a realistic description, especially in view of the asymmetric, nonlinear response of the individual filaments. Thus, a more microscopic model is needed (*SI Text*).

Our work suggests that mechanisms of self-organization in motor-filament systems are not strictly universal, but depend on the biophysical characteristics of both filaments and motors. This nonuniversality is biologically relevant: the physiological function of microtubule arrays differs from that of actin arrays. Microtubules form well-focused mitotic spindle poles, to accomplish high-fidelity separation of the duplicated chromosomes (2). In contrast, actomyosin aggregates appear in cells from diverse tissues and organisms as transient structures that coalesce into larger arrays that exert contractile forces. Examples include the formation of contractile rings driving cytokinesis (3, 4) and wound healing (23), and the formation of contractile networks driving deformation of epithelial cell layers in developing embryos (24–26) and polarizing cortical flows (5, 6). Our findings suggest that the formation and subsequent coalescence of myosin foci in vivo can emerge spontaneously from physical interactions between actin filaments and motors. However, Rho-mediated signaling events certainly contribute to the localized assembly and activation of myosin alongside with purely biophysical effects by changing myosin's phosphorylation state (47). Localized Rho zones for instance lead to localized assembly of active myosin foci in the cleavage furrow (20, 48) and in wound borders (23). Interestingly, the size of the actomyosin condensates in vitro is comparable to the size of condensates observed in vivo (Table S3). It will be interesting to test the activity of purified nonmuscle myosins in our assay. Muscle and nonmuscle myosins differ in duty ratio, sliding velocity, and filament size (Table S1). Nonmuscle myosin IIB is substantially more processive than muscle myosin II, which should suppress the dissolution of actomyosin condensates and enhance the late stages of coalescence. Nonmuscle myosins also have a substantially smaller sliding velocity than muscle myosin II, which should reduce the coalescence rate.

Even though our reconstituted assay mimics self-organized structures and dynamics of actomyosin in cells, there is an important difference. Our in vitro structures are irreversible once assembled, whereas cellular structures dissolve and reform on time scales of minutes. The low (0.1 mM) ATP level in the in vitro assay compared to the typical mM ATP level in nonmuscle cells may contribute to the enhanced stability of the structures. This low level was a prerequisite for active coarsening by skeletal muscle myosin II. At mM ATP concentrations, we did not observe active contractility (Fig. S1*D*) in line with prior studies (12, 13). We attribute this ATP dependence to the low duty ratio of skeletal muscle myosin II. With excess ATP, the duty ratio is only 4%, but lowering the ATP concentration to 100 μM increases the duty ratio about fourfold (12, 13, 49). In addition to the different ATP level, multiple factors that cause dynamic remodeling in cells are absent in our assay. Disassembly will likely require actin depolymerization and monomer recycling. The actin filaments in our experiments were not stabilized and were, thus, in a state of constant treadmilling. Nonetheless, this treadmilling process is very slow (50) and stabilization of actin with phalloidin indeed did not change the self-organization process (Fig. S6*A*). However, cells contain protein factors that accelerate depolymerization or sever F-actin. It will be interesting to incorporate some of these regulators in our assay (51). Another contribution to fast pattern renewal in cells may be the transient nature of physiological actin-cross-linking proteins. Notably, a recent in vitro study of actin networks bundled with fascin showed that myosin could spontaneously disassemble contractile structures (40). There may be an interplay between myosin force production and force-induced dissociation of cross-link proteins that controls the lifetime of cellular contractile structures (52, 53). Finally, assembly of cellular actomyosin condensates into ordered structures such as contractile rings depends not only on myosin contractility but also on forces produced by actin disassembly (23, 54).

Conclusion

We have shown that myosin motors organize actin filaments into contracted states through a multistage aggregation process. We propose a physical mechanism that can account for this process based on motor-induced buckling in connected actin structures. The fact that the reconstituted system is able to mimic cellular self-organized states and their contractile dynamics suggests that physical interactions contribute to the regulation of cell and tissue morphogenesis.

Material and Methods

Preparation of Actomyosin Networks. Myosin synthetic filaments were formed at room temperature by dilution of myosin II in 25 mM imidazole buffer (pH 7.4) with 300 mM KCl to 70 mM KCl. Actomyosin network formation was initiated by adding monomeric G-actin and transferring the samples to glass flow

cells (25 μm depth) at room temperature. The assembly buffer had final concentrations of 25 mM Imidazole-HCl (pH 7.4), 50 mM KCl, 2 mM $MgCl_2$, 1 mM DTT, and contained 0.1 mM MgATP. An enzymatic ATP regeneration system was included and 2 mM Trolox was added to prevent photobleaching. The average length of the actin filaments measured by fluorescence microscopy was 6 μm ($N = 3711$). The actin network was fluorescently labeled with AlexaFluor488-actin, and myosin was labeled with DyLight 488 or 594. Cross-links were created by copolymerizing actin with Biotin-G-actin and adding streptavidin. Details on protein purification and labeling, network reconstitution, and atomic force microscopy (AFM) imaging of myosin filaments are given in the *SI Text, Materials and Methods*.

Fluorescence Microscopy. Samples were imaged within 5 min after mixing with a spinning disk confocal microscope (CSU22, Yokogawa Electric Corp.) on a DMIRB Leica inverted microscope. The sample was excited with 561 nm laser light (Melles Griot) or 488 nm laser light (Coherent Inc.). Images were recorded with a cooled EM-CCD camera (C9100, Hamamatsu Photonics) using an exposure time of 50–100 ms. Image stacks were obtained by scanning through the z-direction in steps of 100 nm with a piezo-driven 100× (1.3 NA) oil immersion objective (PL Fluotar Leica).

Image Analysis. To determine the size of actin condensates, we binarized 8-bit images in Image J (http://rsbweb.nih.gov/ij/) and measured the major radius of each feature using the "Measure" command. Data are shown as averages ± S.D. Kymographs were made with the Kymograph plugin for Image J by J. Rietdorf (Friedrich Miescher Institute Basel, Switzerland) and A. Seitz (European Molecular Biology Laboratory, Heidelberg, Germany).

ACKNOWLEDGMENTS. We thank S. Duineveld, M. Kuit-Vinkenoog, and I. Piechocka with help in protein purification and M. Gardel and M. Lenz for discussions. This work is part of the research program of the Foundation for Fundamental Research on Matter, which is financially supported by the Netherlands Organisation for Scientific Research (NWO).

1. Howard J (2001) *Mechanics of Motor Proteins and the Cytoskeleton* (Sinauer, Sunderland, MA).
2. Karsenti E, Vernos I (2001) The mitotic spindle: A self-made machine. *Science* 294:543–547.
3. Vavylonis D, Wu J, Hao S, O'Shaughnessy B, Pollard T (2008) Assembly mechanism of the contractile ring for cytokinesis by fission yeast. *Science* 319:97–100.
4. Moores S, Sabry J, Spudich J (1996) Myosin dynamics in live Dictyostelium cells. *Proc Natl Acad Sci USA* 93:443–446.
5. Hird S, White J (1993) Cortical and cytoplasmic flow polarity in early embryonic cells of Caenorhabditis elegans. *J Cell Biol* 121:1343–1355.
6. Mayer M, Depken M, Bois JS, Julicher F, Grill SW (2010) Anisotropies in cortical tension reveal the physical basis of polarizing cortical flows. *Nature* 467:617–621.
7. Surrey T, Nedelec F, Leibler S, Karsenti E (2001) Physical properties determining self-organization of motors and microtubules. *Science* 292:1167–1171.
8. Nédélec FJ, Surrey T, Maggs AC, Leibler S (1997) Self-organization of microtubules and motors. *Nature* 389:305–308.
9. Hentrich C, Surrey T (2010) Microtubule organization by the antagonistic mitotic motors kinesin-5 and kinesin-14. *J Cell Biol* 189:465–480.
10. Urrutia R, McNiven MA, Albanesi JP, Murphy DB, Kachar B (1991) Purified kinesin promotes vesicle motility and induces active sliding between microtubules in vitro. *Proc Natl Acad Sci USA* 88:6701–6705.
11. Karsenti E, Nédélec F, Surrey T (2006) Modelling microtubule patterns. *Nat Cell Biol* 8:1204–1211.
12. Humphrey D, Duggan C, Saha D, Smith D, Kas J (2002) Active fluidization of polymer networks through molecular motors. *Nature* 416:413–416.
13. Smith D, et al. (2007) Molecular motor-induced instabilities and cross-linkers determine biopolymer organization. *Biophys J* 93:4445–4452.
14. Koenderink GH, et al. (2009) An active biopolymer network controlled by molecular motors. *Proc Natl Acad Sci USA* 106:15192–15197.
15. Janson E, Kolega J, Taylor D (1991) Modulation of contraction by gelation/solation in a reconstituted motile model. *J Cell Biol* 114:1005–1015.
16. Mizuno D, Tardin C, Schmidt CF, MacKintosh FC (2007) Nonequilibrium mechanics of active cytoskeletal networks. *Science* 315:370–373.
17. Bendix PM, et al. (2008) A quantitative analysis of contractility in active cytoskeletal protein networks. *Biophys J* 94:3126–3136.
18. Strzelecka-Golas Zewska H, Piwowar U, Pliszka B (1981) Changes in the ultrastructure of actomyosin gel during hydrolysis of ATP under various ionic conditions. *Eur J Cell Biol* 24:116–123.
19. DeBiasio R, LaRocca G, Post P, Taylor D (1996) Myosin II transport, organization, and phosphorylation: Evidence for cortical flow/solation-contraction coupling during cytokinesis and cell locomotion. *Mol Biol Cell* 7:1259–82.
20. Werner M, Munro E, Glotzer M (2007) Astral signals spatially bias cortical myosin recruitment to break symmetry and promote cytokinesis. *Curr Biol* 17:1286–1297.
21. Verkhovsky A, Svitkina T, Borisy G (1995) Myosin II filament assemblies in the active lamella of fibroblasts: their morphogenesis and role in the formation of actin filament bundles. *J Cell Biol* 131:989–1002.
22. Verkhovsky A, Borisy G (1993) Non-sarcomeric mode of myosin II organization in the fibroblast lamellum. *J Cell Biol* 123:637–652.
23. Mandato C, Bement W (2001) Contraction and polymerization cooperate to assemble and close actomyosin rings around Xenopus oocyte wounds. *J Cell Biol* 154:785–797.
24. Blanchard GB, Murugesu S, Adams RJ, Martinez-Arias A, Gorfinkiel N (2010) Cytoskeletal dynamics and supracellular organisation of cell shape fluctuations during dorsal closure. *Development* 137:2743–2752.
25. Franke J, Montague R, Kiehart D (2005) Nonmuscle myosin II generates forces that transmit tension and drive contraction in multiple tissues during dorsal closure. *Curr Biol* 15:2208–2221.
26. Martin A, Kaschube M, Wieschaus E (2008) Pulsed contractions of an actin-myosin network drive apical constriction. *Nature* 457:495–499.
27. Rauzi M, Verant P, Lecuit T, Lenne P (2008) Nature and anisotropy of cortical forces orienting Drosophila tissue morphogenesis. *Nat Cell Biol* 10:1401–1410.
28. Astrom JA, Kumar PBS, Karttunen M (2009) Aster formation and rupture transition in semi-flexible fiber networks with mobile cross-linkers. *Soft Matter* 5:2869–2874.
29. Kruse K, Joanny J, Julicher F, Prost J, Sekimoto K (2004) Asters, vortices, and rotating spirals in active gels of polar filaments. *Phys Rev Lett* 92:078101.
30. Ziebert F, Zimmermann W (2005) Nonlinear competition between asters and stripes in filament-motor systems. *Eur Phys J E Soft Matter* 18:41–54.
31. Lee H, Kardar M (2001) Macroscopic equations for pattern formation in mixtures of microtubules and molecular motors. *Phys Rev E Stat Nonlin Soft Matter Phys* 64:056113.
32. Gittes F, Mickey B, Nettleton J, Howard J (1993) Flexural rigidity of microtubules and actin filaments measured from thermal fluctuations in shape. *J Cell Biol* 120:923–934.
33. Vicente-Manzanares M, Ma X, Adelstein RS, Horwitz AR (2009) Non-muscle myosin II takes center stage in cell adhesion and migration. *Nat Rev Mol Cell Biol* 10:778–790.
34. Footer MJ, Kerssemakers JWJ, Theriot JA, Dogterom M (2007) Direct measurement of force generation by actin filament polymerization using an optical trap. *Proc Natl Acad Sci USA* 104:2181–2186.
35. MacKintosh F, Levine A (2008) Nonequilibrium mechanics and dynamics of motor-activated gels. *Phys Rev Lett* 100:018104.
36. Kruse K, Julicher F (2003) Self-organization and mechanical properties of active filament bundles. *Phys Rev E Stat Nonlin Soft Matter Phys* 67:051913.
37. Lau A, Hoffmann B, Davies A, Crocker J, Lubensky T (2003) Microrheology, stress fluctuations, and active behavior of living cells. *Phys Rev Lett* 91:198101–198104.
38. Huxley H (1963) Electron microscope studies on the structure of natural and synthetic protein filaments from striated muscle. *J Mol Biol* 7:281–308.
39. Pepe F, Drucker B (1979) The myosin filament. VI. Myosin content. *J Mol Biol* 130:379–393.
40. Backouche F, Haviv L, Groswasser D, Bernheim-Groswasser A (2006) Active gels: Dynamics of patterning and self-organization. *Phys Biol* 3:264–273.
41. Brangwynne C, Koenderink G, Mackintosh F, Weitz D (2008) Nonequilibrium microtubule fluctuations in a model cytoskeleton. *Phys Rev Lett* 100:118104.
42. Schaller V, Weber C, Semmrich C, Frey E, Bausch AR (2010) Polar patterns of driven filaments. *Nature* 467:73–77.
43. Sankararaman S, Menon G, Kumar P (2004) Self-organized pattern formation in motor-microtubule mixtures. *Phys Rev E Stat Nonlin Soft Matter Phys* 70:031905.
44. Eisenberg M, Guy R (1979) A proof of the hairy ball theorem. *Am Math Mon* 86:571–574.
45. Liverpool T, Marchetti M (2003) Instabilities of isotropic solutions of active polar filaments. *Phys Rev Lett* 90:138102.
46. Verkhovsky A, Svitkina T, Borisy G (1997) Polarity sorting of actin filaments in cytochalasin-treated fibroblasts. *J Cell Sci* 110:1693–1704.
47. Tan JL, Ravid S, Spudich JA (1992) Control of nonmuscle myosins by phosphorylation. *Annu Rev Biochem* 61:721–759.
48. Zhou M, Wang Y (2007) Distinct pathways for the early recruitment of myosin II and actin to the cytokinetic furrow. *Mol Biol Cell* 19:318–326.
49. Finer J, Simmons R, Spudich J (1994) Single myosin molecule mechanics: Piconewton forces and nanometre steps. *Nature* 368:113–119.
50. Kuhn JR, Pollard TD (2005) Real-time measurements of actin filament polymerization by total internal reflection fluorescence microscopy. *Biophys J* 88:1387–1402.
51. Pantaloni D, Clainche CL, Carlier M (2001) Mechanism of actin-based motility. *Science* 292:1502–1506.
52. Reichl EM, et al. (2008) Interactions between myosin and actin cross-linkers control cytokinesis contractility dynamics and mechanics. *Curr Biol* 18:471–480.
53. Wilson CA, et al. (2010) Myosin II contributes to cell-scale actin network treadmilling through network disassembly. *Nature* 465:373–377.
54. Carvalho A, Desai A, Oegema K (2009) Structural memory in the contractile ring makes the duration of cytokinesis independent of cell size. *Cell* 137:926–937.

Supporting Information

Silva et al. 10.1073/pnas.1016616108

SI Materials and Methods

Materials. Monomeric (G-) actin and myosin II were purified from rabbit psoas skeletal muscle without column purification (1, 2). G-actin was stored at −80 °C in G-buffer (2 mM Tris-HCl, 0.2 mM Na_2ATP, 0.2 mM $CaCl_2$, 0.2 mM dithiothreitol (DTT), 0.5 mM NaN_3, pH 8.0). Myosin II was stored at −20 °C in a high-salt buffer with glycerol (0.6 M KCl, 25 mM KH_2PO_4, 10 mM EDTA, 1 mM DTT, pH 6.5, 50% w/w glycerol). Fresh myosin solutions were prepared daily by dialysis against AB300 buffer (300 mM KCl, 4 mM $MgCl_2$, 1 mM DTT, 25 mM imidazole, pH 7.4). Protein concentrations were determined by absorption measurements at 280 nm for myosin and 290 nm for G-actin, using extinction coefficients of 0.53 cm^2/mg for myosin and 1.1 cm^2/mg for G-actin, respectively (1). G-actin labeled with biotin was purchased from Cytoskeleton (Tebu Bio), and G-actin labeled with Alexa488 or Alexa568 was purchased from Invitrogen. Streptavidin was obtained from Pierce (Thermo Fischer), and creatine phosphate (CP) and creatine kinase (CK) were obtained from Roche Diagnostics. Other chemicals were purchased from Sigma Aldrich. ATP was prepared as a 100 mM MgATP stock solution using equimolar amounts of Na_2ATP and $MgCl_2$ in a 10 mM imidazole-HCl buffer (pH 7.4).

Fluorescent Labeling of Myosin II Motor Proteins. Myosin II was labeled with DyLight NHS Ester 488 or 594 (Perbio) according to a protocol adapted from refs. 3 and 4. This labeling preserves the reversible assembly of myosin into synthetic filaments and its actin-activated MgATPase activity. All procedures were performed at 4 °C. Myosin was first assembled into synthetic filaments by a 2 h dialysis against a low-salt buffer (10 mM Hepes, 50 mM KCl, 0.2 mM EGTA, 2 mM MgATP, 2 mM $MgCl_2$, pH 7.0). To the clear top layer of the dialyzed myosin, a 20-fold molar excess of the fluorescent dye (from a 40 mM stock in dimethylsulfoxide) was slowly added. After incubation on ice and in the dark for 1 h, the labeling reaction was stopped by addition of 20 mM D-Lysine. Unreacted dye was removed by dialyzing the myosin solution for at least 3 h against a buffer containing 10 mM Hepes, 50 mM KCl, and 0.2 mM EGTA at pH 7.0. After addition of 10 mM $MgCl_2$, the fluorescent myosin filaments were precipitated by centrifugation for 10 min at 8,000 g. The pellets were resuspended in a minimal volume of high-salt buffer favoring filament disassembly (600 mM KCl, 50 mM KH_2PO_4, 1 mM DTT, pH 7.5) and the solution was dialyzed against the same buffer overnight. Aggregates were removed by centrifugation (10 min at 8000 g). We obtained labeling stoichiometries between 1.7 and 2.7 dye molecules per myosin molecule, based on the ratio between the absorbance at 280 nm and the absorbance of the dye at its maximum. The labeled myosin was stored at −20 °C in monomeric form in a high-salt buffer with glycerol (600 mM KCl, 50 mM KH_2PO_4, 1 mM DTT, pH 7.5 with 50% glycerol).

Actomyosin Network Reconstitution. Reconstituted networks were prepared in assembly buffer with final concentrations of 25 mM imidazole-HCl, 50 mM KCl, 0.1 mM MgATP, 2 mM $MgCl_2$, 1 mM DTT, and pH 7.4. To prevent ATP depletion, we included a regeneration mixture containing 11.76 mM creatine phosphate, 766 units/mL creatine kinase (5). To prevent photobleaching, we added 2 mM Trolox. The actin concentration was fixed at 23.8 μM (1.0 mg/mL). The average length of the actin filaments measured by fluorescence microscopy and analysis of 3,711 filaments was 6 μm (analyzed using the NeuronJ plugin of ImageJ). The actin network was labeled by mixing fluorescent G-actin and unlabeled actin in a 1:20 molar ratio. We inserted a controlled number of cross-link points into the actin filaments by copolymerizing biotinylated G-actin with unlabeled G-actin in a molar ratio varying from zero to 1:20. The number of available cross-link points per actin filament is about 14 at the highest biotin density, assuming that cross-link points occur in equally probable random placement along the filaments. Excess streptavidin (streptavidin:actin molar ratio of 1:25) was included to form cross-links between the biotinylated actin filaments. The molar ratio between myosin and actin was varied between 1:300 and 1:50. For all samples myosin was mixed with all buffers first, allowing the formation of synthetic filaments at room temperature. Finally, G-actin was added and the sample was quickly transferred to a flow cell composed of a glass slide and coverslip separated by a 25 μm FEP spacer (fluorinated ethylene propylene copolymer, Goodfellow) and closed with silicone grease (Baysilone, GE Bayer). The final structure of the patterns was unaffected when myosin monomers were added last to the polymerizing actin. However, this mixing sequence slowed the process of active coalescence down. Actin polymerization did not seem to affect the self-organization process: a fully formed actin network was present before any spatial inhomogeneities in actin or myosin density appeared. Rheology experiments suggested that network formation was complete within about 30 min (Fig. S4*B*). As a further test that actin polymerization has no influence on self-organization, we mixed myosin filaments with preformed actin filaments, and indeed found the same final contracted states (Fig. S6*B*).

Assembly and Characterization of Myosin Synthetic Filaments. The low-salt conditions of the assembly buffer induce the spontaneous assembly of myosin by its tail-region into synthetic filaments (6). Structural studies using electron microscopy (EM) showed that these filaments are structurally homologous to native thick filaments in muscle in terms of bipolarity and subunit periodicity (7). The filaments consist of a central bare zone where the myosin molecules are antiparallel, flanked on both sides by a parallel array of myosin motors with a crown of 3 myosin molecules every 14.3 nm. We determined the length distribution of the myosin filaments by atomic force microscopy (AFM) imaging of myosin filaments assembled for 5 min at room temperature at a concentration of 0.1 μM in the same assembly buffer used for networks. The assembled filaments were pipetted into freshly cleaved mica surfaces coated with nitrocellulose. The samples were imaged by AFM using a Veeco Dimension 3100 atomic force microscope (Veeco) in tapping mode with tips of the type MPP-12100-10 (Veeco). The filament length and diameter were measured using WSxM software (Nanotec). The diameter was obtained as the average of the filament height determined across a profile along the filament contour.

Contractility from Asymmetric Load Response. Perhaps surprisingly, microscopically polar, directed motor activity can give rise to net contractility even in macroscopically apolar structures, provided that the load response is asymmetric. Individual actin filaments are highly asymmetric in their response on the micrometer scale, in that they strongly resist extension, yet buckle easily under compressive loads of less than a piconewton. We approximate this load response as that of an inextensible macroscopic rope with zero resistance to compression. For networks of such actin filaments cross-linked on the micrometer scale, the network load response is also expected to be asymmetric. On this scale, such networks are inhomogeneous with loose or floppy regions that

we refer to as rope-like structures (RLS). These are analogous to a macroscopic fishnet, which resists extension, but crumples or compresses easily. Such a RLS then supports tensile loads but no compressive loads. This means that only attractive/contractile forces can result from interactions mediated through such a structure.

To illustrate how net contractility can arise from motors interacting with a RLS, we consider the following simple problem. Being random networks, RLS are apolar: at any given point in space, they are likely to have actin filaments of random orientation. Thus, when a motor binds to the RLS, its motion can be regarded as a random walk with a step length that is expected to be small if the motors are nonprocessive. We first consider two random walkers (RWs) that are rigidly coupled together; e.g., in a large myosin aggregate (see Fig. S5*A*, *Upper*), as we find in stage 2 of myosin driven actin reorganization (see Fig. 4 of main text). These are allowed to interact with an idealized RLS (Fig. S5*A*, *Lower*) that is assumed to be inextensible, but to buckle under the slightest compressive load.

The probability distribution for the contour length s between the RWs—kept a fixed distance $x = l$ apart—satisfies

$$\frac{\partial P(s,t)}{\partial t} = D\frac{\partial^2 P(s,t)}{\partial s^2}, \quad s > l,$$
$$P(s,0) = 2\delta(s-l), \quad \frac{\partial P(l,t)}{\partial s} = 0.$$

The diffusion constant $D = \Delta s^2/(2\Delta t)$ is set by the step size Δs and stepping time Δt for the RWs. The resulting spreading half Gaussian

$$P(s,t) = \frac{e^{-(s-l)^2/(4Dt)}}{\sqrt{\pi D t}}, \quad s > l,$$

gives the average amount of the rope pulled in between the RWs as a function of time

$$\langle s(t)\rangle - l = \sqrt{4Dt/\pi}.$$

The contraction is diffusive, and acts best over short distances. This idealized case where an asymmetric load response leads to contraction over time could be generalized to more realistic situations describing, for example, myosin filaments in a focus interacting with a disordered actin network structure (see Fig. S5*A*, *Upper*). With a bias, which could be thought of as capturing the network turnover bridging parts of buckled structures, the rate of contraction would remain finite also over large distances. The unbiased model of Fig. S5*A* is numerically realized 10 times in Fig. S6*B*, starting with $s = l = 100\Delta s$.

We next consider the case of RWs that are not connected, but interact dissipatively through the background (see Fig. S5*C*)—mimicking, for example, two myosin foci both interacting with the same buckle prone actin structure and a dissipative background network (corresponding to stage 3 in Fig. 4 of the main text). Simultaneous pulling on a taut structure will bring the walkers together whereas simultaneous compression will make the RLS buckle and arc-length will be gathered in between the RWs while they remain fixed in space. This asymmetry drives the RWs together over time. According to the above, the contour length between the RWs performs a random walk, while the distance between RWs tracks the minimum distance attained by this random walk up to the present time (see Fig. S5*D*). The probability over the contour distance s again satisfies the diffusion equation

$$\frac{\partial P(s,t)}{\partial t} = D\frac{\partial^2 P(s,t)}{\partial s^2}.$$

The transition-time distribution $\Psi(\tau,\Delta x)$ for taking the step in real space $x \to x + \Delta x$, starting with a taut rope $x = s$, can be calculated as

$$\Psi(\tau,\Delta x) = \frac{\Delta x e^{-\Delta x^2/(4Dt)}}{4\sqrt{\pi D}\tau^{3/2}}.$$

The distribution of transition times is broad, with a wide-tail falling off as $1/\tau^{3/2}$. The average time to take a step forward diverges in this model, indicating that the dynamics is highly irregular with long pauses to contraction. The average velocity remains positive

$$\langle v\rangle = \langle \Delta x/\tau\rangle = \int_0^\infty d\tau(\Delta x/\tau)\Psi(\tau,\Delta x) = D/\Delta x,$$

showing the possibility of rapid contraction over short distances. This simple model can be extended to the situation with multiple RLS connecting the RWs. Here, the distance between RWs would track the minimum contour length attained in any one of the multiple diffusion processes. In Fig. S5*E* we show an example of an experimentally measured time evolution of the distance between the two contracting myosin foci shown in Movie S13. The motion is clearly directional, but seems interspersed by pauses of apparent inactivity—as is the case for the simple model presented here.

These simple examples show idealized cases where an asymmetric load response of the material connecting the motors results in an overall net contraction. We could further consider more complex material responses, allowing for reversible and irreversible deformations of the background network and the RLS. The limits we have considered assume the existence of floppy portions of the network with slack that can be "pulled-out." Whereas this is expected to be the case for realistic networks, it is not captured by the largely continuum mechanical models that have been used to date to model these networks, usually on larger scales. To the extent that continuum linear elasticity applies, the mechanism we propose would not result in contractility. Continuum mechanics, however, is unlikely to describe well the relatively loose meshwork of filaments expected for our system at the microscopic scale of a few microns.

1. Pardee J, Spudich J (1982) Purification of muscle actin. *Methods Enzymol* 85:164–181.
2. Margossian S, Lowey S (1982) Preparation of myosin and its subfragments from rabbit skeletal muscle. *Methods Enzymol* 85:55–71.
3. DeBiasio R, Wang L, Fisher G, Taylor D (1988) The dynamic distribution of fluorescent analogues of actin and myosin in protrusions at the leading edge of migrating Swiss 3T3 fibroblasts. *J Cell Biol* 107:2631–45.
4. Kolega J (1998) Fluorescent analogues of myosin II for tracking the behavior of different myosin isoforms in living cells. *J Cell Biochem* 68:389–401.
5. Mizuno D, Tardin C, Schmidt CF, MacKintosh FC (2007) Nonequilibrium mechanics of active cytoskeletal networks. *Science* 315:370–373.
6. Koretz J (1982) Hybridization and reconstitution of thick-filament structure. *Methods Enzymol* 85(Pt B):20–55.
7. Huxley H (1963) Electron microscope studies on the structure of natural and synthetic protein filaments from striated muscle. *J Mol Biol* 7:281–308.

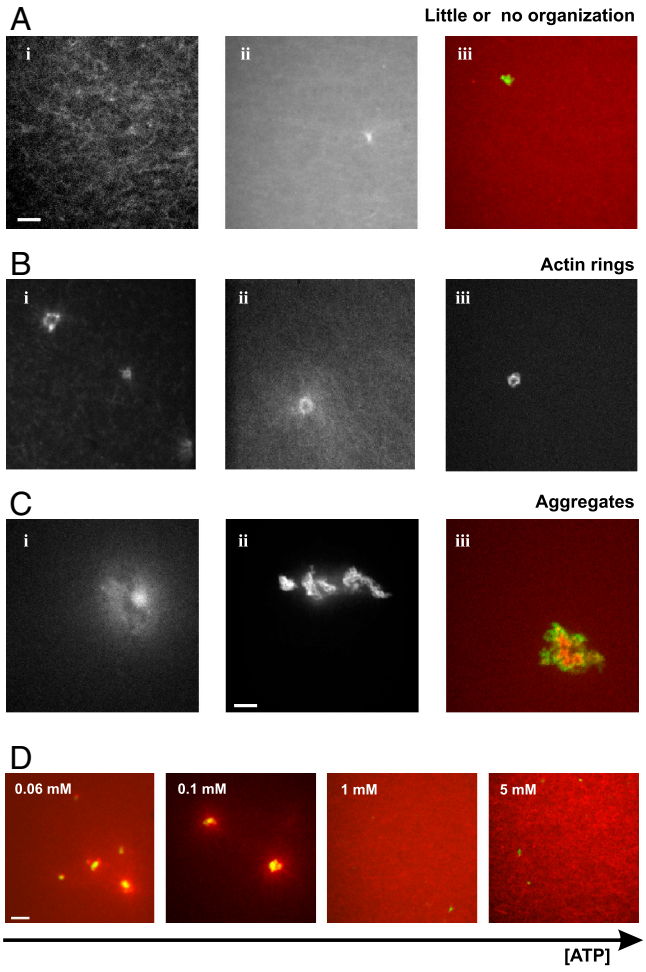

Fig. S1. Myosin processivity affects in vitro actin active organization. (*A–C*) Minifilaments of skeletal myosin II assembled at 150 mM KCl are seldom able to reorganize actin networks. (*A*) Fluorescent micrographs of active networks with labeled actin (*i*, *ii*) and doubly labeled with actin in red and myosin in green (*iii*). In the presence of myosin II minifilaments, networks often remain overall homogenous without evidence of active foci formation. (*B*) Fluorescent micrographs of active networks with labeled actin. Rings rarely emerge in actin networks in the presence of minifilaments. (*C*) Fluorescent micrographs of active networks with labeled actin (*i*, *ii*) and doubly labeled with actin in red and myosin in green (*iii*). Often, disordered aggregates appear in the network. Scale bar, 5 μm. All fields of view are the same size except (*C ii*) where the scale bar is 10 μm. (*D*) ATP concentration modulates pattern formation in active actin-myosin networks. Fluorescence micrographs of actomyosin networks (actin in red and myosin in green) taken at different ATP concentrations. At levels of 60–100 μM ATP, myosin is sufficiently processive to cause the formation of actomyosin condensates. In contrast, the actin network remains homogeneous and the myosin filaments remain homogeneously dispersed in the network at mM ATP concentrations, indicating that myosin is not sufficiently processive to cause network reorganization. Scale bar, 5 μm. Samples from panels *A–D* contain 1:200 myosin:actin and the crosslinker:actin ratio is 1:1,000.

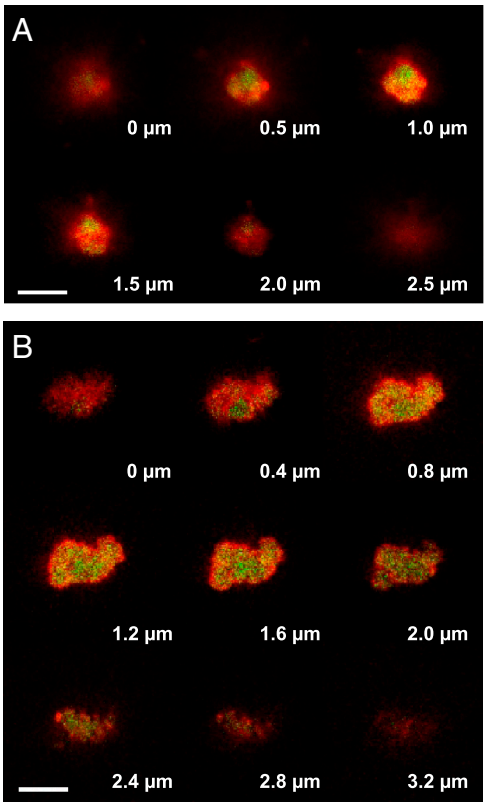

Fig. S2. Stack of confocal microscopy x-y slices of fluorescently labeled actin-myosin condensates (myosin in green and actin in red). Scale bars, 5 μm. (*A*) Sequence of xy-slices of an actomyosin condensate at 1:200 motor:actin ratio. Myosin is in the center, and an actin shell surrounds it. (*B*) Sequence of xy-slices of a superaggregate composed of several actomyosin condensates at 1:50 motor:actin ratio. Each myosin focus within the condensate is surrounded by a shell of actin.

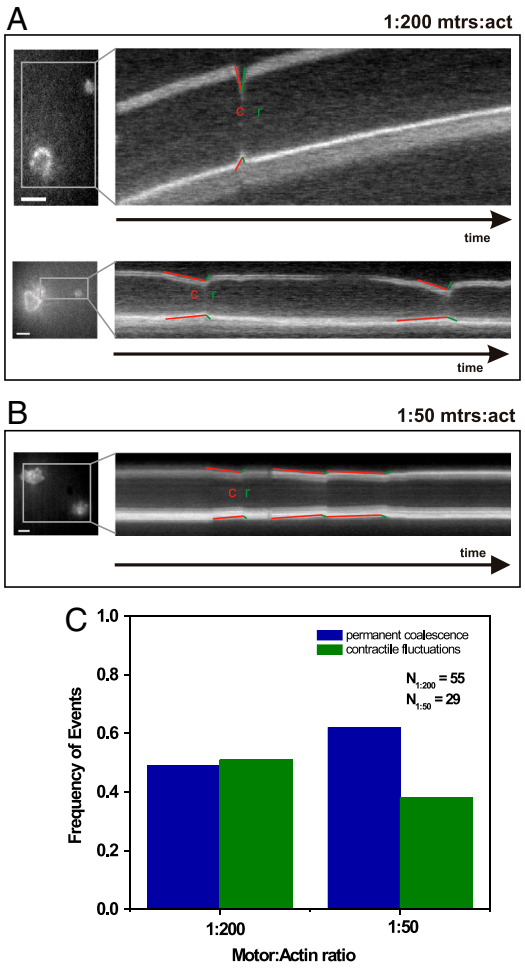

Fig. S3. Myosin concentration influences the dynamics of actin network contractility. (*A* and *B*) Snapshots of actomyosin condensates (labeled actin only) with corresponding kymographs of contractile fluctuation events. Red lines indicate contracting period (*c*) and green lines indicate relaxation/recoil (*r*). Scale bars, 5 μm. (*A*) (*Upper*) Two ring-like actin structures move toward each other and relax. Total kymograph duration 612 s. (*Lower*) Two small actin structures move toward each other and relax two consecutive times. Total kymograph duration 133 s. The crosslinker:actin ratio is 1:1,000 and the myosin:actin ratio is 1:200. (*B*) Two large actin structures slowly move toward each other and then relax three consecutive times. Total kymograph duration 154 s. The crosslinker:actin ratio is 1:1,000 and the myosin:actin ratio is 1:50. (*C*) Statistics of permanent coalescence versus contractile fluctuation events of actomyosin condensates in actin-myosin networks as a function of myosin:actin molar ratio.

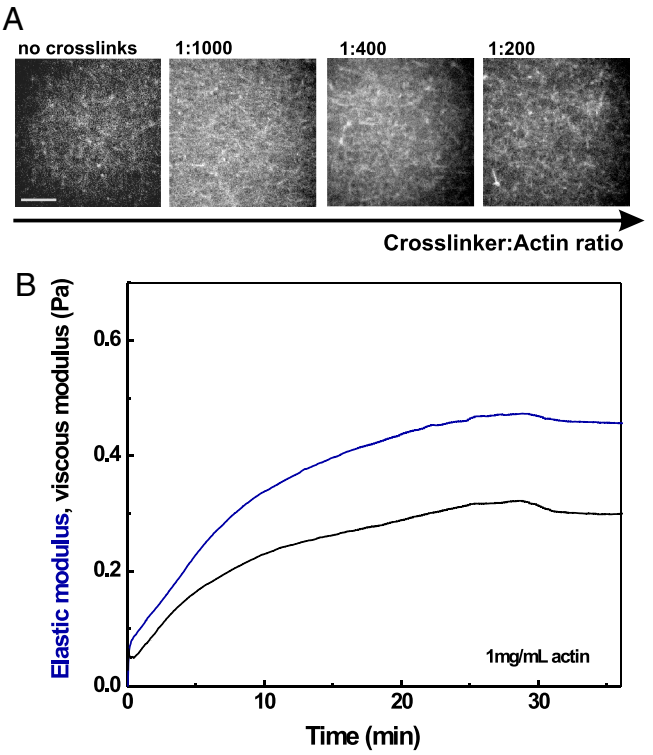

Fig. S4. Passive actin network formation. (*A*) Fluorescence micrographs of passive actin networks (no myosin) with different cross-linker (biotin-actin) densities. Cross-linking does not change the overall network structure up to a concentration of 0.12 μM (at an actin concentration of 23.8 μM). Above this threshold, the network structure looks somewhat coarser, but no distinct aligned or ordered patterns are visible. Actin was polymerized in the presence of 50 mM KCl, 2 mM $MgCl_2$ and 100 μM MgATP. Scale bar, 10 μm. (*B*) Polymerization curve of a passive actin network (no myosin) at 1 mg/mL at 25 °C, obtained by measuring the elastic and viscous shear moduli in a stress-controlled rheometer (Anton Paar MCR501), using oscillatory shear with a small strain amplitude of 0.5%. The curves are averages of four independent experiments using stainless steel CP20-1 and PP20 geometries.

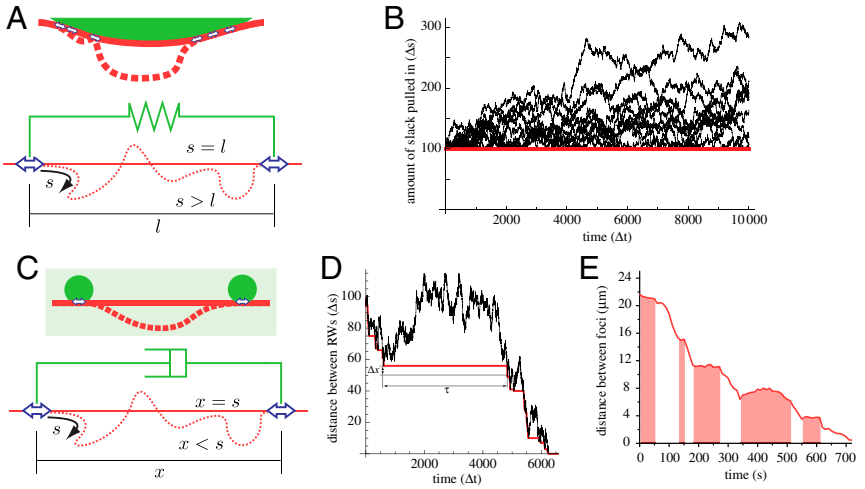

Fig. S5. (*A*) The random rope-like structures (RLS) can either be taut (solid red) or buckled (dotted red) between the random walkers (blue arrows). On top we illustrate a RLS interacting with a larger aggregation of random walkers (RWs) such as present in myosin foci. Below is the idealized model with only two rigidly coupled (green) RWs. Though the walkers are able to push in slack between themselves they are unable to extend a taut RLS. (*B*) The amount of RLS contour length between the walkers, *s*, performs a random walk reflected at $s = l$ (RLS is taut). Here we show time traces for 10 different realizations, all starting at $s = l = 100\Delta s$. (*C*) The RLS can either be taut (solid red) or buckled (dotted red) between the random walkers (blue arrows). On top we illustrate two myosin foci immersed in a viscous background and interacting with a buckle prone network structure. Below we show the simplified model describing this situation. The walkers are unaffected by the viscosity coupling them together through the background network (green dash-pot). When the RW both stochastically pull on an already taut RLS it brings the RWs together. Though the viscous coupling is assumed weak enough not to hinder the motors, it is assumed to be strong enough to induce buckling as soon as the rope is put under compression by the motors. If the RWs randomly compress the RLS, it buckles as material is fed in between the RWs. This excess material has to be pulled-out before the RLS can be made taut and move the RWs closer in space. (*D*) In black we show a numerical realization of the diffusion of the contour length, and in red the corresponding distance between the RWs. (*E*) Experimentally measured distance between the two contracting myosin foci shown in Movie S13. Shaded areas indicate regions where the connecting structure may be under compression, rendering the foci immobile.

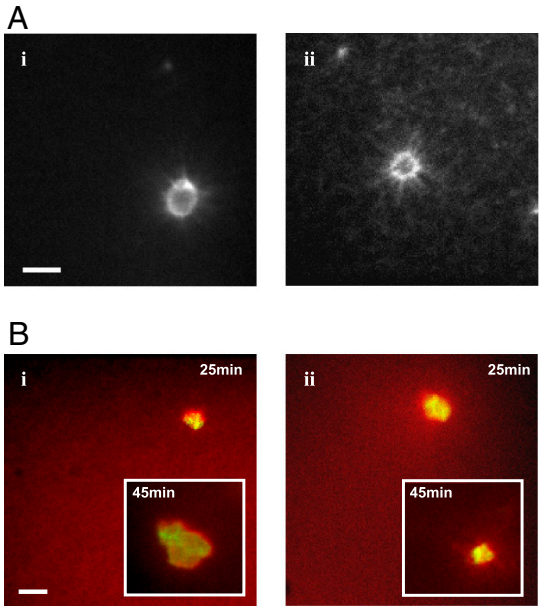

Fig. S6. Active pattern formation in actomyosin networks is not affected by actin dynamics. (*A*) Stabilizing actin filaments does not alter the multistage coarsening process. (*i*) Fluorescent micrograph of a network of labeled actin and unlabeled myosin filaments (myosin : actin ratio is 1 : 200) 35 min after polymerization in the presence of phalloidin (phalloidin : actin molar ratio is 1 : 1). Image shows example of a ring-like actin structure with a size of about 5 μm. The cross – linker : actin ratio is 1 : 1,000. Scale bar, 5 μm. (*ii*) Fluorescent micrograph of control network without phalloidin. (*B*) Mixing preformed actin filaments with myosin filaments does not alter the multistage coarsening process. (*i*) Fluorescent micrograph of a network of labeled actin filaments and myosin filaments (myosin : actin ratio is 1 : 200) 25 min after mixing. Image shows example of an actin/myosin condensate with a size of approximately 4 μm. Scale bar, 5 μm. (*Inset*) Example of a condensate 45 min after mixing. The cross – linker : actin ratio is 1 : 1,000. (*ii*) Fluorescent micrograph of control network 25 min after mixing of preformed myosin filaments with monomeric actin. (*Inset*) Example of a condensate 45 min after mixing.

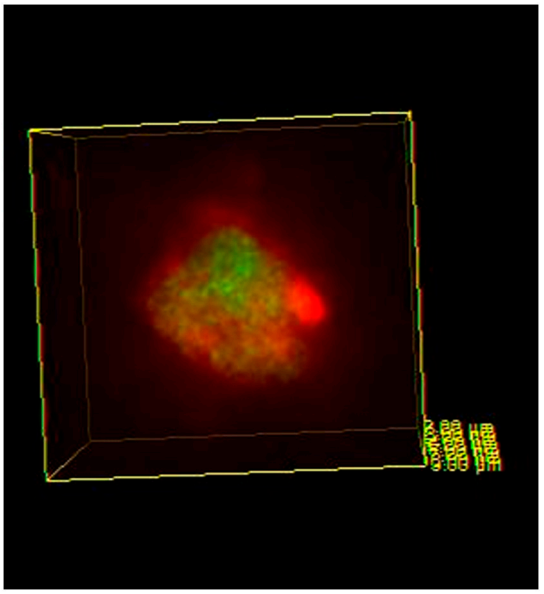

Movie S1. Reconstruction of a 3D stack of 40 fluorescence images of an actin/myosin condensate formed in stage 2 of the multistage coarsening process, obtained using confocal microscopy. Actin (shown in red) accumulates in a dense, disordered shell all around the surface of a globular myosin aggregate (shown in green). The cross – linker : actin ratio is 1 : 1,000 and the myosin : actin ratio is 1 : 200. Corresponding 2D slices are shown in Fig. S2*A*.
Movie S1 (AVI)

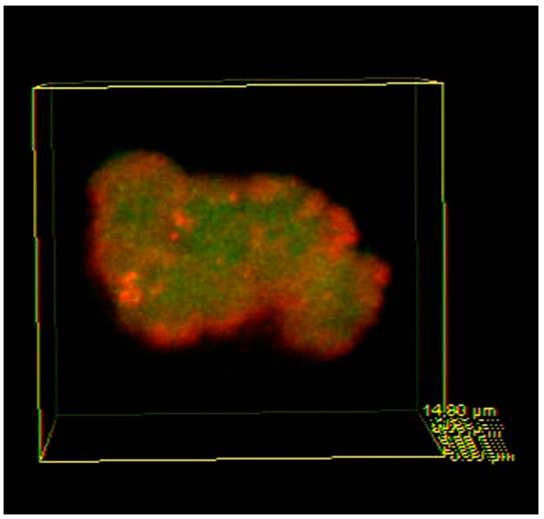

Movie S2. Reconstruction of a three-dimensional stack of 50 fluorescence images of a superaggregate of multiple actin (red)/myosin (green) condensates formed in stage 3 of the multistage coarsening process, obtained using confocal microscopy. The cross – linker : actin ratio is 1 : 1,000 and the myosin : actin ratio is 1 : 50. Corresponding 2D slices are shown in Fig. S2*B*.

Movie S2 (AVI)

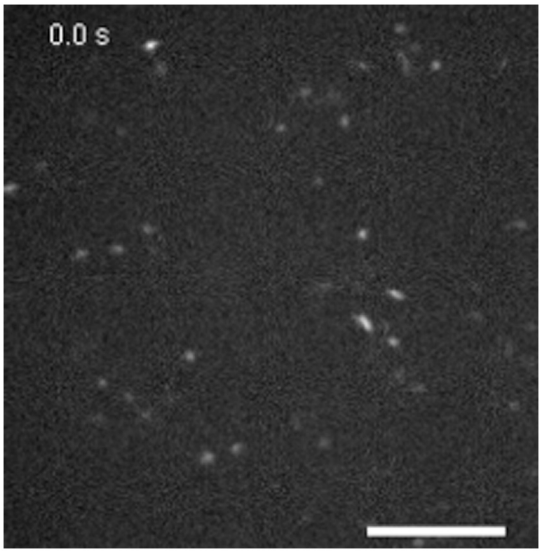

Movie S3. Fluorescently labeled myosin filaments are initially homogeneously distributed throughout the actin network (actin not labeled). In the first 5 min after sample preparation (stage 1 of the multistage coarsening process), they move in an apparently diffusive fashion either through the mesh or actively in a preferred direction, presumably walking along actin filaments. Myosin filaments that meet sometimes fuse into small aggregates. No cross-linkers were added and the myosin : actin ratio is 1 : 300. White arrows represent examples of active walks. Movie total duration is 110 s, 10× real frame rate. Scale bar is 10 μm.

Movie S3 (AVI)

Movie S4. Cropped region of Movie S3, where two fluorescently labeled myosin filaments (or small aggregates thereof) fuse upon meeting. Movie total duration is 55 s, 5× real frame rate. Scale bar is 5 μm.

Movie S4 (AVI)

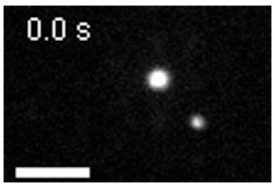

Movie S5. At the beginning of stage 2 of the multistage coarsening process, two myosin foci in an unlabeled actin network abruptly and permanently coalesce with each other as a result of network contractility. The larger one is virtually immobile whereas the small one suddenly approaches and merges with it. The cross – linker : actin ratio is 1 : 1,000 and the myosin : actin ratio is 1 : 200. Movie total duration is 45 s, 5× real frame rate. Scale bar is 5 μm.
Movie S5 (AVI)

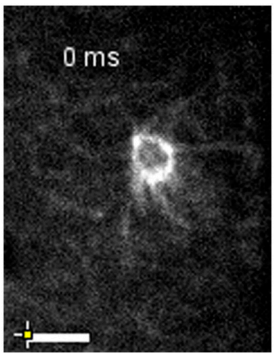

Movie S6. During stage 2 of the multistage coarsening process, a ring-like actin pattern incorporates a fragment of the surrounding actin network (indicated by the white arrow; note that myosin is not labeled). The cross – linker : actin ratio is 1 : 1,000 and the myosin : actin ratio is 1 : 200. Movie total duration is 12 s, 3× real frame rate. Scale bar is 5 μm.
Movie S6 (AVI)

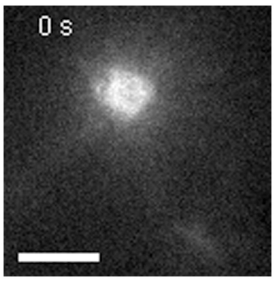

Movie S7. An actin condensate incorporates multiple fragments of the surrounding actin network (myosin is not labeled). The cross – linker : actin ratio is 1 : 1,000 and the myosin : actin ratio is 1 : 200. White arrows represent examples of network fragments being dragged in by the actin ring-like pattern. Movie total duration is 12.3 min, 50× real frame rate. Scale bar is 10 μm.
Movie S7 (AVI)

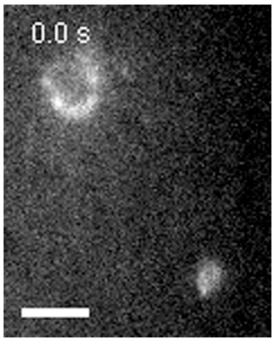

Movie S8. Example of a contractile fluctuation event, where two actin ring-like structures move toward each other and suddenly relax (myosin is not labeled). The parallel white arrows indicate the movements toward and away from each other. The cross – linker : actin ratio is 1 : 1,000 and the myosin : actin ratio is 1 : 200. Movie total duration is 52 s, 10× real frame rate. Scale bar is 10 μm.

Movie S8 (AVI)

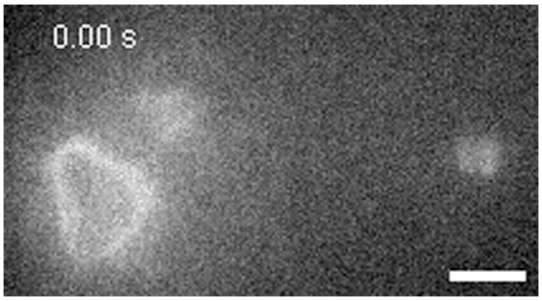

Movie S9. Example of a repeated contractile fluctuation event, where two small actin ring-like structures move toward each other and slowly relax two consecutive times (myosin is not labeled). White circles indicate the beginning of active events. The cross – linker : actin ratio is 1 : 1,000 and the myosin : actin ratio is 1 : 200. Movie total duration is 117 s, 5× real frame rate. Scale bar is 5 μm.

Movie S9 (AVI)

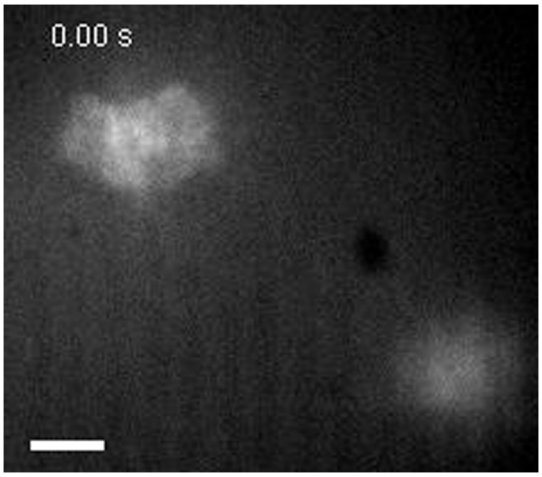

Movie S10. Example of a repeated contractile fluctuation event, where two large actin structures move toward each other and slowly relax three consecutive times (myosin is not labeled). White circles indicate the beginning of active events. No cross-linkers were added. The myosin : actin ratio is 1 : 50. Movie total duration is 104 s, 5× real frame rate. Scale bar is 5 μm.

Movie S10 (AVI)

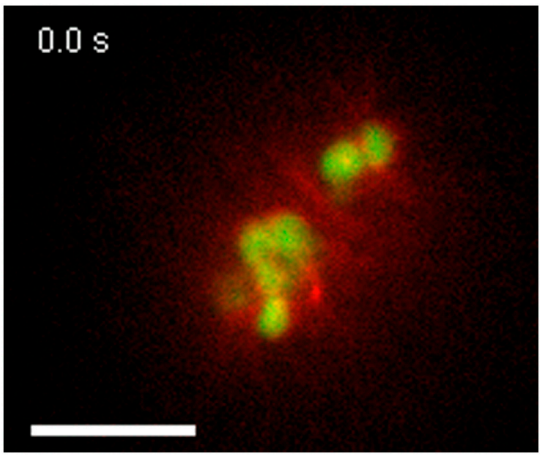

Movie S11. Example of a permanent coalescence event, where two actin (red)/myosin (green) condensates coalesce and crumple the actin network between them. The cross – linker : actin ratio is 1 : 1,000 and the myosin : actin ratio is 1 : 200. The white arrow represents an actin network fragment (in red) that becomes compressed in between the two structures. Movie total duration is 62 s, 10× real frame rate. Scale bar is 10 μm.
Movie S11 (AVI)

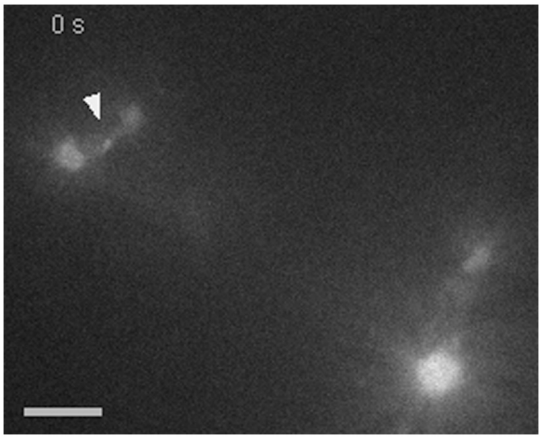

Movie S12. Actin cables form in an actin/myosin network due to contractility. Several actin/myosin condensates appear to be momentarily connected by bundle-like actin structures that collapse when foci approach each other or after foci walk along and drag them. The cross – linker : actin ratio is 1 : 1,000 and the myosin : actin ratio is 1 : 200. White arrows represent examples of such cables emerging. Movie total duration is 22.7 min, 100× real frame rate. Scale bar is 10 μm.
Movie S12 (AVI)

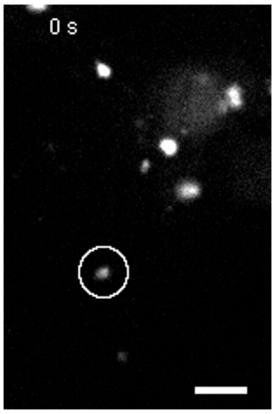

Movie S13. Example of a myosin focus coalescing in an intermittent fashion with a cluster of foci. The cross – linker : actin ratio is 1 : 1,000 and the myosin : actin ratio is 1 : 200. The white circle indicates the focus moving toward the cluster in formation. Movie total duration is 16.5 min, 100× real frame rate. Scale bar is 5 μm.

Movie S13 (AVI)

Table S1. Different class II myosins have distinct kinetic behaviors

Organism	V_{max} (s^{-1})	K_{ATPase} (μM)	Sliding velocity (μm/s)	Duty ratio (%)
		Skeletal muscle myosin II		
Rabbit	86.1 (1)	14 (1)	2.5* (2)	Approximately 4 (3)
Chicken			4.6† (2)	
		Nonmuscle myosin IIA		
Human	0.17 (4)	72 (4)	0.29 (5)	Approximately 5 (4)
		Nonmuscle myosin IIB‡ (6)		
Human	0.13	59	0.05	23
		Nonmuscle myosin II-C‡ (7)		
Mouse	0.16	4.6	0.04	—
		Smooth muscle myosin II		
Chicken	0.7 (8)	59 (8)	0.58 (3)	Approximately 4 (3)

Summary of literature values for the kinetic parameters of actin-activated MgATPase activity of various types of myosin II. Buffer conditions in which variables were measured are indicated together with the literature reference.

ATPase assay: 4 mM Imidazole, 4 mM $MgCl_2$, 10 mM KCl, 1 mM DTT, 1 mM NaN_3, 3 mM NaATP, pH 7.0, 37 °C (1). In vitro motility: 25 mM Imidazole, 1 mM EGTA, 4 mM $MgCl_2$, 1 mM DTT, 25 mM KCl, 1 mM ATP, pH 7.4, 30 °C (2). In vitro motility: 25 mM Imidazole, 1 mM EGTA, 4 mM $MgCl_2$, 10 mM DTT, 1 mMATP, pH 7.4 30 °C (3). ATPase assay: 10 mM 3-(N-morpholino)propanesulfonic acid (MOPS), 0.15 mM EGTA, 2 mM $MgCl_2$, pH 7.0, 25 °C (4). In vitro motility: 20 mM MOPS, 0.1 mM EGTA, 5 mM $MgCl_2$, 80 mM KCl, 1 mM ATP, pH 7.4, 30 °C (5). ATPase assay: 10 mM MOPS, 0.15 mM EGTA, 2 mM $MgCl_2$, 1 mM ATP, pH 7.0, 25 °C (6). ATPase assay: 20 mM MOPS, 0.1 mM EGTA, 2 mM $MgCl_2$, 0.2 mM $CaCl_2$, 1 mM ATP, pH 7.0, 25 °C . In vitro motility: 20 mM MOPS, 50 mM KCl, 0.1 mM EGTA, 5 mM $MgCl_2$, 1 mM ATP, 50 mM DTT, pH 7.4, 30 °C (7). ATPase assay: 5 mM Tris, 1 mM EGTA, 1 mM $MgCl_2$, 10 mM KCl, 0.2 mM $CaCl_2$, 1 mM ATP, pH 7.0, 25 °C (8).

*ATP (0.1 mM).

†ATP (1 mM).

‡Nonspliced isoforms NMII-B0 and C0.

1 Reniscow D, Deacon JC, Warrick HM, Spudich JA, Leinwand LA (2010) Functional diversity among a family of human skeletal muscle myosin motors. *Proc Natl Acad Sci USA* 107:1053–1058.

2 Toyoshima YY, Kron SJ, Spudich JA (1990) The myosin step size: Measurement of the unit displacement per ATP hydrolyzed in an in vitro assay. *Proc Natl Acad Sci USA* 87:7130–7134.

3 Harris DE, Warshaw DM (1993) Smooth and skeletal muscle myosin both exhibit low duty cycles at zero load in vitro. *J Biol Chem* 268:14764–14768.

4 Kovács M, Wang F, Hu A, Zhang Y, Sellers JR (2003) Functional divergence of human cytoplasmic myosin II: kinetic characterization of the nonmuscle IIA isoform. *J Biol Chem* 278:38132–38140.

5 Wang F, Harvey EV, Conti MA, Wei D, Sellers JR (2000) A conserved negatively charged amino acid modulates function in human nonmuscle myosin IIA. *Biochemistry* 39:5555–5560.

6 Wang F, et al. (2003) Kinetic mechanism of nonmuscle myosin IIB: Functional adaptations for tension generation and maintenance. *J Biol Chem* 278:27439–27448.

7 Jana SS, et al. (2009) An alternatively spliced isoform of nonmuscle myosin II-C is not regulated by myosin light chain phosphorylation. *J Biol Chem* 284:11563–11571.

8 Marston SB, Taylor EW (1980) Comparison of the myosin and actomyosin ATPase mechanisms of the four types of vertebrate muscles. *J Mol Biol* 139:573–600.

Table S2. Quantification of the size of actomyosin condensates observed in active networks containing varying concentrations of myosin motors (compare to Fig. 3*B*) and biotin-streptavidin cross-linkers (compare to Fig. 3*C ii*), and quantification of contraction speeds of coalescing condensates (compare to Fig. 3*C i*)

Fig 3B

Motor:actin ratio	⟨Size⟩ (μm)	SD (μm)	N		
1:300	1.75	±0.72	27		
1:200	2.36	±1.14	18		
1:50	5.34	±4.08	39		
ANOVA test	df	SS	MS	F	*P*
Model	2	239	119	14.4	4.3×10^{-6}
Error	81	669	8.3	-	-
Total	83	808	-	-	-

$P \ll 0.001$: populations are significantly different.

Fig 3Ci—speed

Crosslinker:actin ratio	Speed (μm/s)	SD (μm/s)	N
No cross-linkers	0.10	0.05	3
1:1,000	0.63	0.20	4
1:400	0.51	0.11	2
1:200	0.03	0.02	4

Fig 3C ii—size

Crosslinker:actin ratio	⟨Size⟩ (μm)	SD (μm)	N		
No cross-linkers	2.30	0.91	20		
1:1,000	1.40	0.89	69		
1:400	0.98	0.28	16		
1:200	1.96	0.92	25		
ANOVA test	Degrees of freedom (df)	Sum of squares (SS)	Mean square (MS)	F	*P*
Model	3	22	7.4	10.2	4.4×10^{-6}
Error	126	91	0.7	—	—
Total	129	113	—	—	—

$P \ll 0.001$: Populations are significantly different.

Statistical analyses were performed using the ANOVA test in Origin Pro8.

Table S3. In vivo assembled myosin II foci and foci formed in vitro have a similar size

Organism	Size (μm)	Reported size	Estimated size	Velocity (μm/s)	Reference
		Contractile ring formation			
Saccharomyces pombe	≤0.5–1	no	from Fig. 3*D*	0.03	1
Wound healing					
Xenopus oocyte	1–4	no	from Fig. 7*C*	0.2–5.8	2
		Developing embryos			
Drosophila	≤5	no	from Fig. 3*I*	none reported	3
Drosophila	approximately 1	no	from Fig. 1*A*, *Inset*	none reported	4
Drosophila	0.5–2	no	from Fig. 2*C*	0.043 ± 0.016	5
Cortical flows					
C.elegans	2.21 ± 1.16	yes: Fig. S6*C*	no	0.24 ± 0.04	6

Summary of reported or estimated sizes of myosin II foci in different organisms and in different cellular or developmental stages.

1 Vavylonis D, Wu J, Hao S, O'Shaughnessy B, Pollard T (2008) Assembly mechanism of the contractile ring for cytokinesis by fission yeast. *Science* 319:97–100.
2 Mandato C, Bement W (2001) Contraction and polymerization cooperate to assemble and close actomyosin rings around Xenopus oocyte wounds. *J Cell Biol* 154:785–797.
3 Blanchard GB, Murugesu S, Adams RJ, Martinez-Arias A, Gorfinkiel N (2010) Cytoskeletal dynamics and supracellular organisation of cell shape fluctuations during dorsal closure. *Development* 137:2743–2752.
4 Franke J, Montague R, Kiehart D (2005) Nonmuscle myosin II generates forces that transmit tension and drive contraction in multiple tissues during dorsal closure. *Curr Biol* 15:2208–2221.
5 Martin A, Kaschube M, Wieschaus E (2009) Pulsed contractions of an actin-myosin network drive apical constriction. *Nature* 457:495–499.
6 Mayer M, Depken M, Bois JS, Julicher F, Grill SW (2010) Anisotropies in cortical tension reveal the physical basis of polarizing cortical flows. *Nature* 467:617–621.